Hindawi Publishing Corporation
International Journal of Aerospace Engineering
Volume 2015, Article ID 473926, 8 pages
http://dx.doi.org/10.1155/2015/473926

Research Article

Effect of Interfacial Debonding on the Strength of Composite Structure-Similarity Scale Model for the Wing-Box

Shiyong Sun,[1] Rui Yang,[1] Zibin Yan,[1] and Wei Qian[2]

[1]*Key Laboratory for Precision and Non-Traditional Machining Technology of Ministry of Education, School of Mechanical Engineering, Dalian University of Technology, Dalian 116024, China*
[2]*School of Aeronautics and Astronautics, Dalian University of Technology, Dalian 116024, China*

Correspondence should be addressed to Rui Yang; yangrui@dlut.edu.cn

Received 17 July 2015; Accepted 29 September 2015

Academic Editor: Hamid M. Lankarani

Based on the wing-box structure, a model was established to analyze the strength of the scale model for the composite wing. Firstly, different failure criteria were set to determine damage onset of the components. The continuum damage variables were adopted in the stiffness degradation rule. Secondly, the interface elements were placed along the interface between the beam flange and the skin to investigate the effects of bonding strength on the ultimate load-carrying capacity of the wing-box. The failure modes of the wing-box structure were studied by using the nonlinear finite element method. The effect of flange's width on the strength of wing-box was discussed based on the prediction method. The results indicated that the ultimate load-carrying capacity varied distinctly with the change of flange's width. However, the bonding strength had limited effect on the model strength as the flange's width increases to the critical value. The research methods and results of the study can serve as reference for the strength analysis on the scale model of composite wing as well as the determination of principles adopted in the design of the scale model for wing spar.

1. Introduction

The composite structure-similarity scale model (ComSSM) for the wing is an advanced model used in the wind tunnel test. It can obtain significant design parameters, such as the aircraft flight performance, load distribution, strength check, and structural configuration [1]. As shown in Figure 1(a), ComSSM is similar to the actual airfoil on the topological structure. The main load-carrying structure is composed of skin, spar, and ribs which are made of composite material. The composite material is of high designability, which ensures an accurate ratio between the model and the actual airfoil in terms of dimension, stiffness, and mass so as to meet the requirement of the similarity theory as well as the wind tunnel test.

The cross section of ComSSM is shown in Figure 1(b). The topological structure and the geometry scale dimension should be taken into consideration in structure design. The stiffness characteristics of the model can be controlled accurately by selecting certain material for skin, spar, and ribs and optimizing the geometric parameters [2]. According to such a design method, some tiny components must be employed in the structure, such as the spar flange, to guarantee the accuracy of the stiffness characteristics. Limited by the dimension of the wind tunnel in China, some component width can only be scaled down to about 2-3 mm in 1 : 6 scale. According to the aerodynamic theory, the surface of the model must be smooth enough to avoid the turbulent airflow. Thus, in the assembly of skin, spar, and ribs, bonding method instead of more reliable methods such as screw connection or riveting way is adopted [3]. In this case, the adhesive area between the spar flange and skin is so small, which may prejudice the strength of the model.

The stiffness and strength analysis focus on the wing-box which is the typical structure and the major load bearing part of ComSSM. The wing-box structure and its cross section containing skin, beam, and rib plate are shown in Figure 2. The major concern for structure design of ComSSM is the geometric scale, based on which the equivalent stiffness method is adopted, and then composites of low modulus are

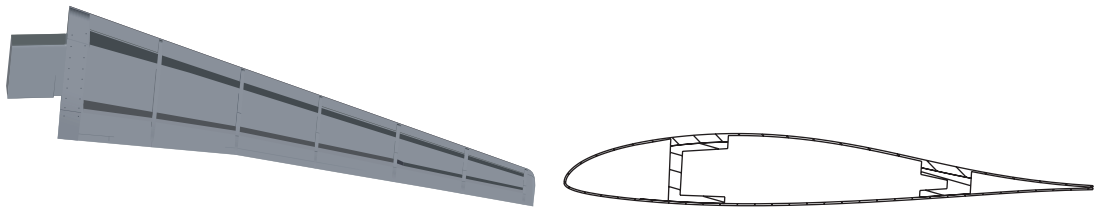

(a) Structure-similarity scale model of composite wing (b) Cross section of the model

Figure 1: Structure-similarity scale model of composite wing and cross section of the model.

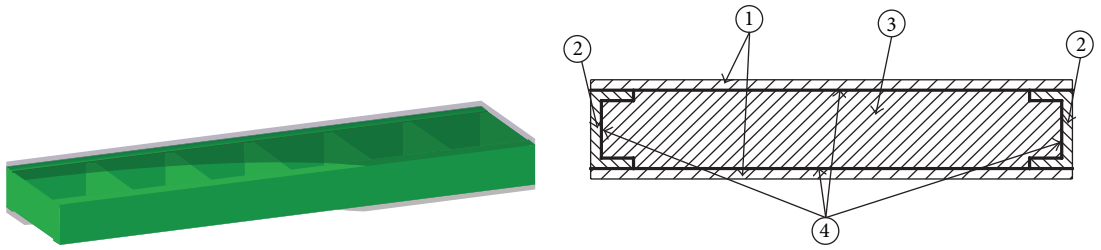

(a) Wing-box structure (b) Wing-box cross section containing ribs

Figure 2: Schematic diagram of composite wing-box. ① Skin. ② C beam. ③ Rib plate. ④ Bonding interface.

employed in manufacturing [4, 5]. During the analysis on the strength of the wing-box, it is usually assumed that the adhesive condition between the wing-box skin and the rib as well as spar is intact. Namely, the interface is strong enough to resist any damage in the test [6, 7]. However, interface debonding occurs easily under the in-plane compression or shear load in the wind tunnel test, for the adhesive area between spar flange and skin is too small. Therefore, it is essential to establish a prediction method to obtain the influence of the spar flange's width on the whole structure strength in the case of ComSSM.

Recently, many scholars have conducted extensive research on interface debonding of composite structures. The interface element method, developed based on the cohesive zone model and theories about damage mechanics and fracture mechanics, has been widely used to study the initiation and propagation of interfacial crack [8]. Thus, it is suitable to be employed in the study on interface mechanical properties of the adhesive joint. Mohammadi et al. [9] proposed a model to predict the progressive damage including the large delamination growth in composite laminates. The model was based on the coupling of continuum damage mechanics with cohesive interface layer. Bouhala et al. [10] investigated crack nucleation and growth in long fiber reinforced composites using the Extended Finite Element Method (XFEM) and the cohesive zone model. Camanho and Dávila [11] analyzed initiation and growth of the interface crack on the stiffened composite plates by using the interface element method. The numerical results were consistent with that of the experiment. Fan et al. [12] adopted the concept of cohesive zone to simulate the delamination in fiber composites and crack growth in adhesive joints in tension or shear fracture modes.

The skin of ComSSM is a typical composite laminated plate, which is characterized by multiple failure modes under load. The traditional composite strength criterion is usually applied to judge the damage initiation. It is assumed that the lamina failure immediately occurs when the load reaches the maximum stress intensity. However, the damage is an evolution process. Sleight [13] introduced the damage process of composite materials by using finite element analysis method. Nowadays, the progressive damage analysis of composite materials is mostly achieved by reducing elastic modulus to simulate the degradation of the materials properties. Usually, the reduction factor is empirical data [14, 15]. To investigate the progressive failure of composites laminates, Chen et al. [16] developed a finite element model including in-ply and delamination damage effects. The cohesive elements available in ABAQUS were employed to simulate delamination behavior in the adhesive interfaces. Liu and Zheng [17] proposed an energy-based stiffness degradation method, based on the Continuum Damage Mechanics (CDM) theory, to predict the progressive failure properties of the Al–carbon fiber/epoxy composite laminates.

In this paper, the finite element model of wing-box is established to analyze the structure strength based on the structure characteristics and manufacturing process of ComSSM. Different failure criteria and materials stiffness degradation model are adopted to represent the materials failure behavior. Interface element method is employed in analyzing the effect of the bonding strength on the bearing capacity of the model. Then the effect of the spar flange's width on the structural strength is studied. The strength prediction method and analysis process would provide theoretical reference for the design of ComSSM.

2. Wing-Box Analysis Model with Interfacial Bonding Strength

2.1. Failure Criterion and Stiffness Degradation of Composite Material. The main component of ComSSM wing-box to bear load is the skin which is a typical composite laminated plate with complex failure modes. As one of the failure criteria, Hashin can distinguish the orientation of the failure and accurately obtain various failure modes of composite material [18]. Firstly, the finite element analysis method is established to calculate the stress on each layer of the composite laminated plate. Then, Hashin's criterion is applied to determine whether material failure occurs on each layer. If failure really occurs according to Hashin's criterion, corresponding stiffness reduction will be made until the material eventually loses its bearing capacity. Specific failure criterion is as follows.

Fiber tensile failure ($\sigma_{11} \geq 0$):

$$e_f^2 = \left(\frac{\sigma_{11}}{X_T}\right)^2 + \alpha\left(\frac{\tau_{12}}{S_L}\right)^2 \geq 1. \quad (1)$$

Fiber crushing failure ($\sigma_{11} \leq 0$):

$$e_f^2 = \left(\frac{\sigma_{11}}{X_C}\right)^2 \geq 1. \quad (2)$$

Matrix tensile failure ($\sigma_{22} \geq 0$):

$$e_m^2 = \left(\frac{\sigma_{22}}{Y_T}\right)^2 + \left(\frac{\tau_{12}}{S_L}\right)^2 \geq 1. \quad (3)$$

Matrix crushing failure ($\sigma_{22} \leq 0$):

$$e_m^2 = \left(\frac{\sigma_{22}}{2S_T}\right)^2 + \left[\left(\frac{Y_C}{2S_T}\right)^2 - 1\right]\frac{\sigma_{22}}{Y_C} + \left(\frac{\tau_{12}}{S_L}\right)^2 \geq 1, \quad (4)$$

where e_f and e_m represent the failure index for fiber and matrix, respectively. X_T and X_C represent the axial tensile and compression strength, respectively. Y_T and Y_C represent the transverse tensile and compression strength, respectively. S_T is transverse shear strength and S_L is the axial shear strength. α is the impact factor of the shear stress on the fiber tensile damage and σ_{11}, σ_{22}, and τ_{12} are effective stress components. The damage operator M is introduced to reduce the stiffness when the material failure occurs. The effective stress $\sigma = M\widehat{\sigma}$, where $\widehat{\sigma}$ is nominal stress. The damage operator M is obtained by

$$M = \begin{bmatrix} \frac{1}{1-d_f} & 0 & 0 \\ 0 & \frac{1}{1-d_m} & 0 \\ 0 & 0 & \frac{1}{1-d_s} \end{bmatrix}, \quad (5)$$

where d_m, d_f, and d_s represent the current state variables of matrix, fiber, and the shear damage on fiber/matrix, respectively. d_s can be also obtained as follows: $d_s = 1 - (1 - d_f)(1 - d_m)$.

Then, the constitutive equation containing damage factor is $\sigma = C_d\varepsilon$, in which

$$C_d = \frac{1}{D}\begin{bmatrix} (1-d_f)E_1 & (1-d_f)(1-d_m)\mu_{21}E_1 & 0 \\ (1-d_f)(1-d_m)\mu_{12}E_2 & (1-d_m)E_2 & 0 \\ 0 & 0 & D(1-d_s)G_{12} \end{bmatrix}, \quad (6)$$

where D can be obtained as follows: $D = 1 - (1 - d_f)(1 - d_m)\mu_{12}\mu_{21}$. Damage state variables are determined by the energy release rate when material damage occurs, which are continuous function of material stress or strain. However, it is difficult to measure all the material's property values. The damage variables d_f and d_m [19] can be calculated as follows:

$$d_j = \min\left\{\lambda, \frac{\langle e_j^2 - \varepsilon\rangle}{1-\varepsilon}\right\}, \quad j = f, m. \quad (7)$$

Here an operator is introduced as follows:

$$\langle a\rangle = \begin{cases} 0, & a \leq 0, \\ a, & a > 0, \end{cases} \quad (8)$$

where the operator in (8) is employed in the calculation of $\langle e_j^2 - \varepsilon\rangle$. $\varepsilon < \lambda < 1$ and ε is close to 1. When the matrix or fiber damage e_j^2 is greater than ε, the material property values begin to decline. d_j increases with the increase of e_j^2, and the maximum value of d_j is λ.

2.2. Failure Criterion and Interface Element for the Adhesive Layer. The interface connects two components of ComSSM and transfers the stress between them. Based on the cohesive zone model, the interface element is introduced to simulate the interface debonding [20]. The interface element which only bears the stress between the adjacent layers is zero thickness; namely, it only withstands normal stress and tangential shear stress; meanwhile the stress in other directions imposed on the interface element is zero. Thus, the constitutive equation of interface element which contains damage factor can be written as follows:

$$\begin{bmatrix} \sigma_{33} \\ \tau_{13} \\ \tau_{23} \end{bmatrix} = (1-d)\begin{bmatrix} E & 0 & 0 \\ 0 & G & 0 \\ 0 & 0 & G \end{bmatrix}\begin{bmatrix} \varepsilon_{33} \\ \gamma_{13} \\ \gamma_{23} \end{bmatrix}, \quad (9)$$

where σ_{33} is the normal stress in Z direction. τ_{13} and τ_{23} represent shear stress in XZ and YZ plane, respectively. d is the damage factor. Quads criterion is adopted to determine the failure criterion of interface element, which is shown as follows [11]:

$$e^2 = \left(\frac{\langle \sigma_{33} \rangle}{X_t}\right)^2 + \left(\frac{\tau_{13}}{S}\right)^2 + \left(\frac{\tau_{23}}{S}\right)^2 \geq 1, \quad (10)$$

where e is the failure index of the interface element and X_t and S represent the interface tensile and shear strength, respectively. Because the interface normal pressure stress has no effects on the sticking-joint crack initiation and extension, $\langle \sigma_{33} \rangle$ is calculated as operator $\langle a \rangle$ mentioned above. Damage variable d is computed by (7); namely, $d = \min\{\lambda, \langle e^2 - \varepsilon \rangle / (1 - \varepsilon)\}$.

2.3. Failure Criterion and Stiffness Degradation of the Spar and Rib. Since the spar and rib of the composite wing-box only bear minor load and enjoy the ply scheme, they can be taken as isotropic material for further analysis. The maximum stress strength theory is adopted in determining the failure criterion; namely, material brittle fracture will occur once the maximum stress reaches critical value of material properties. The corresponding equation is $|\sigma_1| \leq \sigma_b$.

If the failure occurs, the material stiffness reduction will be realized by the user subroutine based on the ABAQUS software. The elastic parameters are reduced to a value that is small enough to meet the destruction characteristics of the brittle material and avoid the direct deletion of the invalid failure elements so as to ensure that the stiffness matrix cannot suffer from singularity and numerical convergence.

3. The Wing-Box Finite Element Model and Analysis Process

3.1. Wing-Box Finite Element Model. A typical example of composite wing-box is shown in Figure 3 with 540 mm in length, 90 mm in width, and 15 mm in height. The width of spar flange is 8 mm. There are 7 ribs placed with equal interval in the wing-box. The left side of the root is the fixed support. In order to simulate the aerodynamic load on the wing-box model in wind tunnel tests, the root stress is determined according to the real aircraft model. Firstly, at the end of the wing-box, several loading points are chosen to get the root stress value. Then, according to the linear superposition principle, the results are compared with the stress at the root of the aircraft model. Finally, the least squares method is employed to inversely confirm the best loading plan. The load imposed at point 1 and point 2 is increased as $F_1 : F_2 = 30 : 1$. Skin, spars, and ribs are all discretized by shell element. The interface element is introduced between the contact area of the skin and spar to simulate the debonding effect on the failure process of the wing-box, as shown in Figure 3. Moreover, the rigid constraints are adopted to ensure the continuity of displacement between the interface element and shell element. The skins are manufactured by unidirectional T300 carbon fiber fabric and low temperature curing epoxy resin. The face layers are layered in $[0/90/45/-45]_s$ configuration with the total thickness of 2 mm. The material properties of laminates are shown in Table 1. The spar and rib are made of the EW100 plain fabric of glass fiber and low temperature curing epoxy resin. The lay stacking is $[(0/90)/(\pm 45)]_{4s}$. The spar and rib are taken as isotropic materials with the elastic modulus $E = 10$ GPa, Poisson's ratio $\mu = 0.31$, and the ultimate strength $\sigma_b = 235$ MPa. The interface layer is made of two-component low temperature curing epoxy structural adhesive, the performance parameters of which are shown in Table 2.

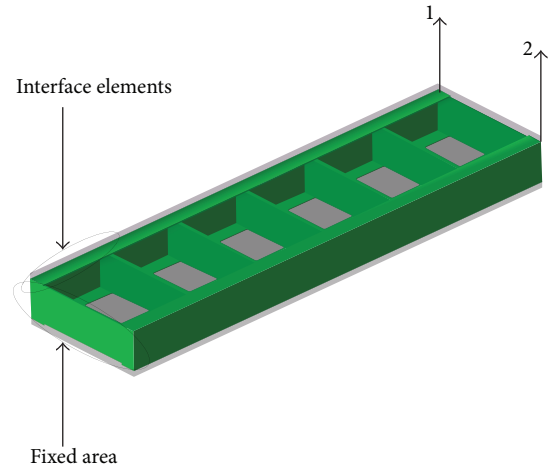

Figure 3: Finite element model of wing-box with bond strength considered.

3.2. Wing-Box Failure Analysis Process. The finite element model is performed in the ABAQUS platform. The constitutive equations of the composite laminates and interface layer are established, respectively. The failure criterion and corresponding stiffness degradation scheme containing the state variables of continuum damage are employed to analyze the failure process. Then, the arc-length method is adopted to solve the nonlinear equations. The flowchart of the analysis is exhibited in Figure 4.

Specific steps are as follows:

(1) Establish the finite element model and give initial load.

(2) Solve the equilibrium equation to obtain all the stress components in each incremental step.

(3) If the failure occurs, calculate the state variables of damage based on the current stress. Then, the finite element equilibrium equations are reestablished according to the reduced material property due to the stiffness degradation. Continue this step until no new damage occurs.

(4) Increase the load ΔP which is imposed on the wing-box. Then repeat step (2) to carry on the next loop until the final failure occurs.

Table 1: Properties of the skin's composite lamina.

The material elastic constants (GPa)				Strength parameters (MPa)				
E_1	E_2	μ_{12}	G_{12}	X_T	X_C	Y_T	Y_C	S
53.3	8.9	0.31	3.45	1050	1050	40	140	50

Table 2: Properties of bonding interface material.

The material elastic constants (GPa)		Strength parameters (MPa)	
E	G	X_t	S
3.4	1.31	51	61

4. Analysis and Discussion on the Example

4.1. Wing-Box Load-Displacement Curve. As an integral component, the wing-box will be identified as reaching the ultimate load once any part of it loses its bearing capacity. The arc-length method is adopted to increase the load step by step. The simulation results show that the upper skin is the first part that suffers the failure, while the spar and rib plate are still undamaged at the same time. Figure 5 illustrates the load-displacement curve of the loading point 1. The dotted line and solid line represent the load-displacement curves with and without taking the spar and skin interface bonding strength into account, respectively.

As shown in Figure 5, the load-displacement curve is linear at first. The state variables show the upper skin initial damage occurs when the load reaches 447.4 N. Then, the load-displacement curve presents the turning point that indicates the material stiffness reduces gradually with the increased load step by step. The increased load causes the element damage evolution until the complete failure occurs. Once the skin failure appears under the bending and torsional loads, the model's loading capacity drops rapidly due to the composite brittleness. When the effect of interface bonding strength is taken into consideration, debonding appears between the skin and spar as the load reaches 820.2 N. The model stiffness and the maximum load decrease more significantly in comparison to the case where interface strength is not considered. The main reason is the fact that the interface debonding affects stress transferring between the skin and the spar, which makes the skins bear more bending load and accelerate the damage evolution. The maximum load value for the model is 925.3 N regardless of the interface strength. However, the maximum load value is 864.4 N for the model when the interface strength is taken into account. Thus, the interface debonding cannot be ignored in the model strength analysis; otherwise the model bearing capacity will be overestimated.

4.2. The Damage Evolution Process. The composite laminates of the skins have various damage modes such as the matrix crushing and the interface debonding which have significant influence on the strength of the overall structure. Therefore, the occurrence and extension of these two modes of damage are mainly discussed in the paper.

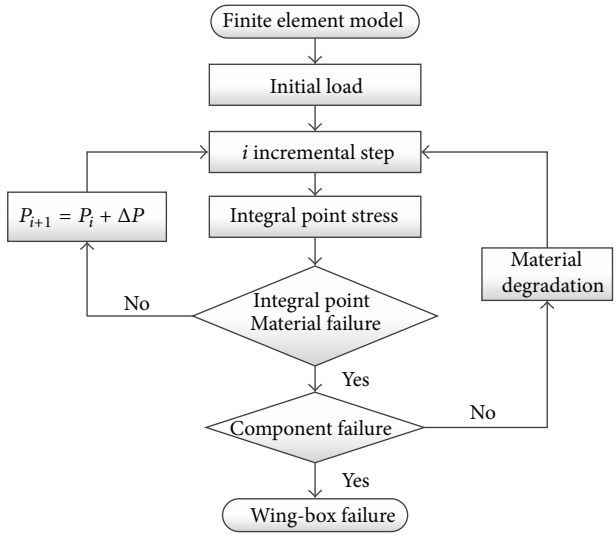

Figure 4: Flow chart of wing-box failure analysis.

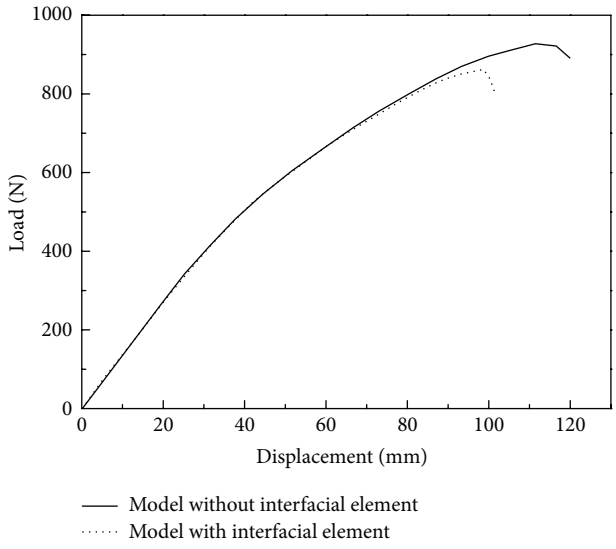

Figure 5: Load-displacement curve of wing-box.

Figure 6 is the diagram of the matrix crushing damage evolution which occurred on the upper skin with 0-degree layer on the top. The light color represents that the materials are damaged and lost their bearing capacity. The matrix damage occurs near the skin root and extends rapidly along the direction of the matrix damage after the load reaches 811.5 N. A variety of damage modes also appear in each of the ply during the damage evolution process. When the load reaches 864.4 N, the upper skin is total failure.

Figure 7 describes the failure process of the interface between the skin and the spar flange. The light color also represents the failure elements which mean the debonded interface. The initial failure occurs along the external contact boundary between the spar flange and skin when the load reaches 820.2 N. The interface shear stress is the main reason behind the debonding and the fracture mode is Mode III type

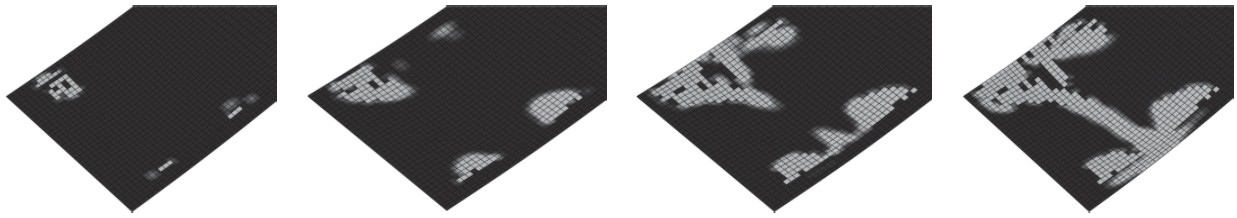

(a) 811.5 N (b) 820.7 N (c) 843.5 N (d) 864.4 N

Figure 6: Matrix damage evolution of the skin.

(a) 820.2 N (b) 833.4 N (c) 847.5 N (d) 864.4 N

Figure 7: Evolution of interface failure.

(tearing mode). The interface normal stress increases gradually with the increased load, which causes the debonding area to expand further. The deformations of the skin and spar are mismatching with each other so that the debonding part of the spar cannot normally transmit the aerodynamic load, which leads the skin to become overloaded and the failure occurs.

4.3. Effect of Flange's Width on the Structure's Ultimate Bearing Capacity. It is generally known that the wing-box is the main bearing structure for the ComSSM. In the wing-box structure, the skin bears the main bending moment. At the same time, the closed box formed by the skin, spar, and rib plate bears the main torque. Although the C spar flange only bears a small part of the bending moment, the change in width will affect the bonding area between the skin and the spar, which means the bonding strength will also be changed. Thus, the effect of the flange's width on the structure's ultimate bearing capacity is worthy of studying, which can help us better understand the ComSSM structure design and reliability research. The ultimate load versus the flange's width with and without the interface debonding behavior is shown in Figure 8. The dash curve and solid curve represent the results with and without interface debonding behavior, respectively.

As shown in Figure 8, without considering the bonding interface strength, the wing-box structure ultimate bearing capacity improves not apparently with the increasing of the width of spar flange. For example, the maximum load with flange's width of 12 mm only increases by 4.5% compared to that of 4 mm. The ultimate bearing capacity of the wing-box structure significantly increases with the increasing of

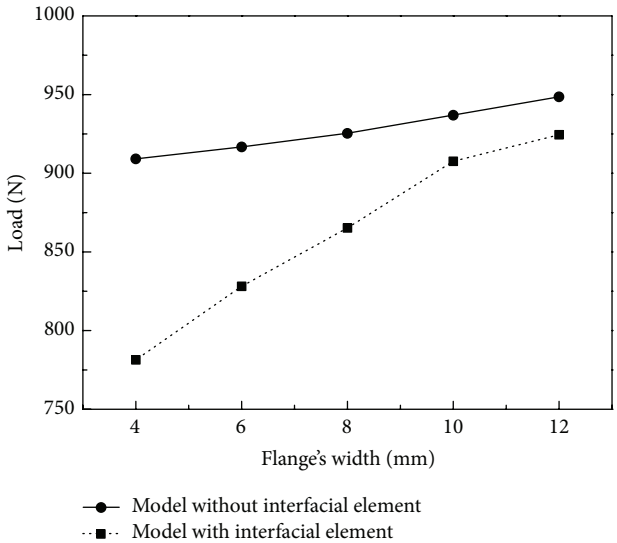

Figure 8: Maximum load versus flange's width curve.

the flange's width for the model that has taken interface bonding strength into account. The corresponding structure maximum load increases by 18.5%. The main reason is the fact that the flange transmits bending and torsion loads and only bears a small part of the bending moment in ComSSM wing-box structure. So mainly failure occurs in skin for the model without taking interface element into consideration and change of the flange's width has little impact on the structural bearing capacity. When the interface elements are placed between the flange and the skin, the interface debonding will be easy to occur at the high stress area of

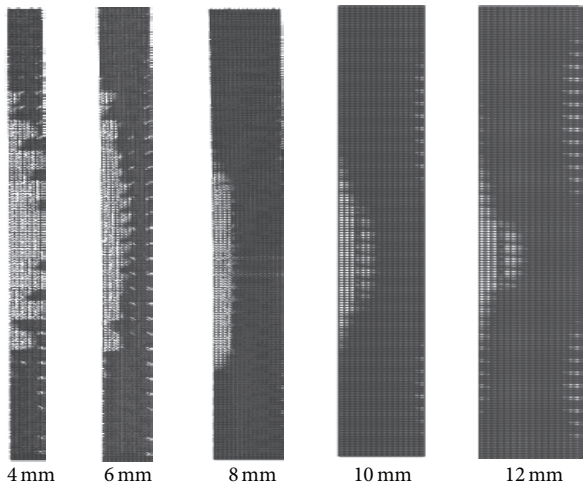

Figure 9: Interface failure diagram under different flange's width.

the root under great bending and torsion loads, especially for the small flange's width. It can worsen the structure load transmitting mechanism and make the skin and the spar deform incompatibly, as a result of which the skin is severely overloaded and the structure failure occurs instantaneously.

The final damage states of the interface elements caused by the ultimate load under different flange's width are shown in Figure 9. It can be seen that the debonding appears on the interface for the flange of 4 mm width. Firstly, the shear stress at the external boundary of the skin and spar leads to the debonding between the skin and the flange. Then, the interface element failures gradually expand to the inner boundary. At the moment, the normal stress caused by the bending load also increases gradually, which accelerates the crack growth until the total failure. The ultimate load for the flange of 4 mm width drops by 14.1% for the model with debonding considered compared to that without debonding considered. The effect of the interface debonding on the bearing capacity of the wing-box decreases gradually with the increasing of the flange's width. For example, the ultimate load only declines by 3.1% and 2.5% for the model with flange of 10 mm and 12 mm width, respectively, caused by the interface debonding. The skin failure occurs before debonding appears on the interface in this situation.

Based on further analysis, it can be concluded that there is a threshold after which the effects of flange's width on the structure strength of the wing-box will begin to decline. The flange with 10 mm width is selected for the model. If the flange's width is less than the threshold, the interface debonding has evident effect on the structure strength. If the flange's width is greater than the threshold, the influence of the interface bonding strength on the structure strength tends to cease. In this case, the influence of the interface debonding can be ignored. Therefore, the influence of the flange's width on structure ultimate strength must be considered to ensure that the model has sufficient strength in the wind tunnel test. Then, the structural topology and size can be optimized so as to keep in line with the similarity theory in the ComSSM design.

5. Conclusion

A finite element model is developed so as to study the effect of the interface bonding strength on the wing-box bearing capacity. Some conclusions can be drawn:

(1) If the interface strength is not considered at high stress concentration area between the skin and the spar, it will overestimate the bearing capacity of the model. Because the skin, rib, and spar are connected together in the adhesive bonding, the interface debonding, which disrupts the transfer of stresses between the skin and spar, occurs easily at the model root under the bending and torsion loads. The analysis indicates that the predicted value of the structure strength between the spar and the skin is obviously lower for the model that takes interface element into account than that for the model that does not take the interface element into account. Thus, it is necessary to consider the effect of the interface debonding on the failure process in ComSSM strength analysis.

(2) For the model with interface element, the structure's ultimate bearing capacity is evidently influenced by the flange's width. The narrower the flange is, the more the structure strength maximum value decreases. It is because the interface debonding breaks the load-transmitting mechanism and leads to the premature failure of the wing-box structure. Conversely, for the model without interface element, the structure strength varies very small as the flange's width changes. In this case, the wing-box bears load as a whole structure, so the variation of flange's width within a certain scope has little influence on the structure strength.

(3) In this study we have also observed a reasonable threshold for the flange's width, within which the width of flange has obvious impact on the structure's bearing capacity. If the flange's width is below the threshold, serious interface debonding and skin premature failure appear. If the flange's width is greater than the threshold, increase of the flange's width has little influence on the improvement of the structure's bearing capacity. However, it will increase the structure's stiffness in this case. Therefore, in the structure design of the ComSSM, it is necessary to carry on the stiffness redistribution based on the threshold.

Conflict of Interests

The authors declare that there is no conflict of interests regarding the publication of this paper.

Acknowledgments

The authors greatly appreciate the financial support of the National Natural Science Foundation of China (nos. 51275073 and 11102032), the Science Fund for Creative Research Groups (no. 51321004), the National Basic Research Program of China

(no. 2014CB046504), and the Fundamental Research Funds for the Central Universities.

References

[1] E. H. Dowell, *A Modern Course in Aeroelasticity*, Springer, Berlin, Germany, 5th edition, 2014.

[2] V. C. Vasily, "Optimization approach to design of aeroelastic dynamically-scaled models of aircraft," in *Proceedings of the 10th AIAA/ISSMO Multidisciplinary Analysis and Optimization Conference*, New York, NY, USA, August-September 2004.

[3] F. Niesiolowski and D. W. Aubrey, "Stress distribution during peeling of adhesive tapes," *The Journal of Adhesion*, vol. 13, no. 1, pp. 87–98, 1981.

[4] W. J. Stroud, T. Krishnamurthy, B. H. Mason et al., "Probabilistic design of a plate-like wing to meet flutter and strength requirements," AIAA A0231150, American Institute of Aeronautics and Astronautics, 2002.

[5] J. Cho and Y. Chang, "Supersonic flutter analysis of wings using an unsteady 3D panel method," *Computers & Fluids*, vol. 30, no. 2, pp. 237–256, 2001.

[6] R. Houlston, "Finite strip analysis of plates and stiffened panels subjected to air-blast loads," *Computers & Structures*, vol. 32, no. 3-4, pp. 647–659, 1989.

[7] P. K. Gotsis, C. C. Chamis, K. David, and F. Abdi, "Progressive fracture of laminated composite stiffened plate," *Theoretical and Applied Fracture Mechanics*, vol. 51, no. 2, pp. 144–147, 2009.

[8] D. Xie and S. B. Biggers Jr., "Progressive crack growth analysis using interface element based on the virtual crack closure technique," *Finite Elements in Analysis and Design*, vol. 42, no. 11, pp. 977–984, 2006.

[9] B. Mohammadi, H. Olia, and H. Hosseini-Toudeshky, "Intra and damage analysis of laminated composites using coupled continuum damage mechanics with cohesive interface layer," *Composite Structures*, vol. 120, pp. 519–530, 2015.

[10] L. Bouhala, A. Makradi, S. Belouettar, H. Kiefer-Kamal, and P. Fréres, "Modelling of failure in long fibres reinforced composites by X-FEM and cohesive zone model," *Composites Part B: Engineering*, vol. 55, pp. 352–361, 2013.

[11] P. P. Camanho and C. G. Dávila, "Mixed-mode decohesion elements for the simulation of delamination in composite materials," NASA/TM 2002-211737, NASA, Washington, DC, USA, 2002.

[12] C. Y. Fan, P.-Y. Ben Jar, and J. J. Roger Cheng, "Cohesive zone with continuum damage properties for simulation of delamination development in fibre composites and failure of adhesive joints," *Engineering Fracture Mechanics*, vol. 75, no. 13, pp. 3866–3880, 2008.

[13] D. W. Sleight, "Progressive failure analysis methodology for laminated composite structures," Tech. Rep. NASA/TP-1999-209107, NASA, Washington, DC, USA, 1999.

[14] F.-K. Chang and L. B. Lessard, "Damage tolerance of laminated composites containing an open hole and subjected to compressive loadings. Part I. Analysis," *Journal of Composite Materials*, vol. 25, no. 1, pp. 2–43, 1991.

[15] P. P. Camanho and F. L. Matthews, "A progressive damage model for mechanically fastened joints in composite laminates," *Journal of Composite Materials*, vol. 33, no. 24, pp. 2248–2280, 1999.

[16] J.-F. Chen, E. V. Morozov, and K. Shankar, "Simulating progressive failure of composite laminates including in-ply and delamination damage effects," *Composites Part A: Applied Science and Manufacturing*, vol. 61, pp. 185–200, 2014.

[17] P. F. Liu and J. Y. Zheng, "Progressive failure analysis of carbon fiber/epoxy composite laminates using continuum damage mechanics," *Materials Science and Engineering A*, vol. 485, no. 1-2, pp. 711–717, 2008.

[18] Z. Hashin, "Failure criteria for unidirectional fiber composites," *Journal of Applied Mechanics—Transactions ASME*, vol. 47, no. 2, pp. 329–334, 1980.

[19] V. K. Goyal, N. R. Jaunky, E. R. Johnson, and D. R. Ambur, "Intralaminar and interlaminar progressive failure analyses of composite panels with circular cutouts," *Composite Structures*, vol. 64, no. 1, pp. 91–105, 2004.

[20] A. Ural, V. R. Krishnan, and K. D. Papoulia, "A cohesive zone model for fatigue crack growth allowing for crack retardation," *International Journal of Solids and Structures*, vol. 46, no. 11-12, pp. 2453–2462, 2009.